

# Tunable Kondo physics in a van der Waals kagome antiferromagnet

Boqin Song<sup>1,2,†</sup>, Yuyang Xie<sup>1,2,†</sup>, Wei-Jian Li<sup>3,†</sup>, Hui Liu<sup>1</sup>, Qinghua Zhang<sup>1</sup>, Jian-gang Guo<sup>1,†</sup>, Lin Zhao<sup>1,2,\*</sup>, Shun-Li Yu<sup>3,\*</sup>, Xingjiang Zhou<sup>1,2</sup>, Xiaolong Chen<sup>1,2,\*</sup>, Tianping Ying<sup>1,†\*</sup>

1. Beijing National Laboratory for Condensed Matter Physics, Institute of Physics, Chinese Academy of Sciences, Beijing 100190, China.
2. School of Physical Sciences, University of Chinese Academy of Sciences, Beijing 100049, China.
3. National Laboratory of Solid State Microstructures and Department of Physics, Nanjing University, Nanjing 210093, China

[\\*lzhao@iphy.ac.cn](mailto:lzhao@iphy.ac.cn)

[\\*slyu@nju.edu.cn](mailto:slyu@nju.edu.cn)

[\\*xlchen@iphy.ac.cn](mailto:xlchen@iphy.ac.cn)

[\\*ying@iphy.ac.cn](mailto:ying@iphy.ac.cn)

## Abstract

**The Kondo lattice physics, describing the hybridization of localized spin matrix with dispersive conduction electrons, breeds numerous discoveries in the realm of strongly correlated quantum matter. Generally observed in lanthanide and actinide compounds, increasing attention has been directed towards alternative pathways for achieving flat band structures, such as Morie superlattices and Kagome metals. However, fine control of Kondo interaction outside of heterostructures remains elusive. Here we report the discovery of a van der Waals (vdW) kagome antiferromagnet CsCr<sub>6</sub>Sb<sub>6</sub>. Angle-resolved photoemission spectra and theoretical analysis show clear flat bands, consisting of half-filled 3d<sub>xz</sub> and 3d<sub>yz</sub> orbitals of Cr, situated 50 meV below the Fermi level. Importantly, we observe the emergence of anomalous Hall effect with remarkable tunability by simple reduction the sample thickness. The effective control of kondo interaction in CsCr<sub>6</sub>Sb<sub>6</sub> render it an ideal platform for exploring unrepresented phenomena using the vast toolkit of vdW structures.**

## Main

The Kondo lattices is one of the prototypes of strongly correlated quantum matter<sup>1-5</sup>. The heavy-fermion phenomenon arising from the exchange interaction between localized magnetic moments and conduction electrons leads to the Kondo lattices physics. At temperature below  $T_K$ , the magnetic moments develop independent singlet with itinerant electrons and are screened gradually. As the temperature further decreases to a coherence scale  $T^*$ , the competition between the Kondo scattering and Ruderman-

Kittel-Kasuya-Yosida (RKKY) interaction drives the system to different ground states from a Kondo Fermi liquid to a magnetic ordered state, as proposed by Doniach<sup>6</sup>. A microscopic understanding of the ground state of the Kondo lattice remains a vital problem especially as more complex scenarios beyond the scope of Doniach were realized, where the Kondo singlet survive in a magnetic ordered ground state. The coexistence and competence of two interactions enable the exploration of quantum criticality, Kondo breakdown and fluctuation-mediated superconductivity. Rare-earth elements are widely used in the construction of Kondo lattice materials. However, their inner compact 4f and 5f orbitals poses a formidable challenge to tuning the electron density and exchange interaction.

The discovery of the Kondo effect in transition metal dichalcogenide (TMD) hetero-bilayers and moiré lattices has recently opened a new pathway for designing Kondo lattices in two-dimensional (2D) systems without f electrons. In these systems, the presence of local moments, stemming from unpaired flat bands near the Fermi energy ( $E_F$ ), resembles Kondo lattices defined by charge density wave (CDW) or moiré superlattices. The prominent advantage of these heterostructure strategies is their excellent compatibility with various interface tuning method such as electrical gating. Kagome materials is another important pathway with intrinsic flat band alongside Dirac points and van Hove singularities due to their unique lattice geometry. The realization of the Kondo effect in Kagome lattices was proposed theoretically for decades, and the experimental clues was found recently in  $Ni_3In$  and  $Mn_3Sn$  with non-Fermi liquid transport and the Kondo resonance, respectively. These findings underscore the role of frustration as a potential driver for strong correlations. However, the inherently three-dimensional (3D) nature of these materials inherently constrains tunability compared to that of superlattices. Hence, the pursuit of exfoliable Kagome materials remains highly desirable for investigating the correlations introduced by the flat band at  $E_F$ .

Here, we present the discovery of a novel Kagome metal  $CsCr_6Sb_6$ , which crystallizes in the hexagonal space group  $R-3m$  (as depicted in Fig. 1b). The lattice parameters are  $a=5.5462$  Å,  $c=34.5280$  Å, and  $V=919.7993$  Å<sup>3</sup>. Detailed synthesis conditions and composition analysis can be found in the Supplementary Information (SI). Fig. 1c illustrates the building blocks of the double-layer  $Cr_6Sb_6$  slab composed of two Kagome lattices shifted along  $[2/3, 1/3, 0]$ . Successive three  $Cr_6Sb_6$  slabs are further shifted through  $[2/3, 1/3, 1/3]$  to form an ABC stacking. X-ray diffraction patterns of the single crystals are shown in Fig. 1d, with their optical image shown in the inset. Additionally, atomic resolved scanning transmission electron microscopy (STEM) imaging along the  $a$ -axis was performed with the crystal structure superimposed.  $CsCr_6Sb_6$  single crystals can be mechanically exfoliated into one-unit-cell layer (1 u.c.  $\sim 3$ nm) as demonstrated in SI. It is also noteworthy that the sample exhibits exceptional robustness against moisture. No discernible differences in transport behavior can be observed even after immersing the fabricated device in water. This property greatly facilitates its future characterization and manipulation.

### **Hallmark of Kondo flat band**

A simple DFT calculation of the band structure of CsCr<sub>6</sub>Sb<sub>6</sub> offers compelling evidence of the anticipated flat bands near the Fermi level (Extended Fig. 1). The band along the  $\Gamma$ -M direction exhibits negligible dispersion, presenting a nearly flat band. In contrast, along the M-K and K- $\Gamma$  directions, the band demonstrates a discernible dispersion with a modest bandwidth of about 250 meV. The flat band along the  $\Gamma$ -M path comes largely from the  $d_{xz}$  and  $d_{yz}$  orbitals, whereas the  $d_{x^2-y^2}$  and  $d_{xy}$  orbitals are primarily responsible for the dispersion band along the M-K and K- $\Gamma$  paths. Additionally, the  $d_{xz}$  and  $d_{yz}$  orbitals are nearly half-filled, whereas the  $d_{x^2-y^2}$  and  $d_{xy}$  orbitals are roughly quarter-filled. This results in an orbital-selective correlation effect, where the  $d_{x^2-y^2}$  and  $d_{xy}$  orbitals contribute itinerant electrons, while the  $d_{xz}$  and  $d_{yz}$  orbitals contribute localized electrons. These conditions create a conducive environment for the emergence of the Kondo effect.

We next employed Angle-Resolved Photoemission Spectroscopy (ARPES) to validate the predicted band structure. Figure 2b depicts the Fermi surface mapping of CsCr<sub>6</sub>Sb<sub>6</sub> measured at 15 K. The typical band structures along high-symmetry directions are illustrated in Fig. 2c,d. A notable discovery is the presence of a nearly dispersionless flat band feature along both  $\Gamma$ -M and  $\Gamma$ -K high symmetry directions of the first Brillouin zone, positioned at 50 meV below the Fermi level. Another prominent feature is a significant gap of approximately 0.5 eV below the flat band feature, spanning from 50 meV to 0.5 eV binding energy. The presence of this sizable gap ensures the formation of a clean flat band which governs the low-energy electronic structure and is solely responsible for the observed physical properties.

To visualize the underlying band structure of the flat band feature more clearly, we plot the energy distribution curves (EDCs) within a smaller energy window by tracing the peaks of EDCs as marked by the red tips in Fig. 2e,f. Now we can see that the flat band feature is not a sole band. There exist two bands around the  $\Gamma$  point. One of them crosses the Fermi level to form a small pocket around Brillouin zone center (as shown in Fig. 1a). Around K point, a flat band crosses Fermi level and forms the triangular pocket. Around M point, the flat band just crosses the Fermi level and forms a strong spot feature on the Fermi surface. This Fermi surface topology is roughly in agreement with the calculated results shown in Fig. 2b. We notice that the band dispersions revealed by LDA calculations and ARPES measurements are not completely consistent, especially along the  $\Gamma$ -K direction. These differences in the band dispersions between the DFT and ARPES results primarily arise from the limitations of DFT calculations to capture the strongly correlated physics related to the Kondo effect. These observations distinguish CsCr<sub>6</sub>Sb<sub>6</sub> from all other reported kagome materials, where the flat band is often mixed with other bands, or positioned far away from the Fermi level.

### **Formation of Kondo singlets**

Electrical transport provides another touchstone for investigating Kondo physics. Figure 3a displays the temperature-dependent resistance of a bulk CsCr<sub>6</sub>Sb<sub>6</sub> sample. It

exhibits metallic behavior at high temperatures and reaches a minimum at 78 K, below which the resistance increases and shows a canonical  $-\ln T$  dependence. This resistance minimum results from enhanced scattering between local moments and itinerant electrons as described by  $\rho = aT^5 + c\rho_0 - c\rho_1 \log T$ . Such scattering simultaneously introduces the RKKY interaction within isolated local moments spin, leading to the formation of antiferromagnetic correlations at proximately  $T_N = 82$  K, as evidenced by the magnetization shown in Fig. 3b.

Unlike scattering from random Kondo impurities, the resistance gradually deviates from the  $-\ln T$  dependence and tends to saturate below  $T_K$  (20 K). Meanwhile, the conductance  $G$  shows a  $T^2$  dependence. This deviation is characteristic of the formation of Kondo singlets, indicating the onset of hybridization between flat bands and the conduction sea. With the population of Kondo singlets gradually overwhelming that of local moments with lowering temperature, it will also significantly influence the magnetoresistance (MR). Figure 3c shows the MR of the bulk sample at different temperatures. At  $T_N$ , a crossover manifests from positive to negative MR, and its amplitude is gradually enhanced with decreasing temperature. The negative MR can be attributed to antilocalization resulting from the suppression of local moments scattering by fields. We plot the amplitude of MR versus temperature at various fields (Fig. 3d). The crossover at  $T_M$  can be clearly seen for all measured magnetic fields. Additionally, the negative MR reaches a maximum at  $T_K$ , below which the renormalized fermions with positive MR resulting from the Kondo hybridization come into play and cancel out the contribution of Kondo singlets. At 2 K, MR remains positive at low field and crosses to a negative one at 8.7 T, indicating the emergence of Kondo destruction when the Zeeman energy exceeds  $k_B T_K$  where  $k_B$  is the Boltzmann constant.

In conventional Kondo lattice, the coherence of Kondo singlets scattering at finite temperature  $T^*$  would drive the system into a heavy fermion liquid ground state, characterized by a significant decrease in resistance. However, the situation becomes more complex in  $\text{CsCr}_6\text{Sb}_6$  as the RKKY interaction also becomes influential, leading to either a drop in resistance or even complete saturation down to 1.8 K. Given that the energy scale of the RKKY interaction  $k_B T_N$  is higher than  $k_B T_K$ , a magnetic ordered ground state naturally emerges. Although we do not observe any anomalous Hall effect in  $R_{xy}$  at 2 K (Fig. 3e), the rise in  $\chi$  below  $T_K$  (Fig. 3b) may be related to the onset of re-localization of the hybridized electrons, serving as a precursor to the antiferromagnetic ordered ground state.

The temperature-dependent resistance behavior, coupled with the magneto-transport properties, provides evidence for the formation of Kondo singlets at  $T_K$  and Kondo destruction at high magnetic fields. The peak of the negative magnetoresistance (MR) and the differential Hall coefficient (Fig. 3f) align with the minimum of  $dR/dT$ , which we will utilize to determine the Kondo temperature and evaluate the energy scale of the Kondo interaction in the following section.

### **Highly tunable Kondo temperature and magnetic ground state**

The vdW nature of CsCr<sub>6</sub>Sb<sub>6</sub> offers opportunities for studying the impact of dimensionality on the Kondo lattice which is impossible to realize in the rare earth compound. Figure 4a shows  $dR/dT$  of different samples with thickness vary from bulk (tens of microns) to 3 nm (1 u.c.). The data are multiplied by different renormalization factors (see raw data in SI) for comparison which do not influence the determination of  $T_K$ . We observe that the  $T_K$  can be feasibly tuned as the thickness is reduced to tens of nanometers, exhibiting a monotonic decrease with the decreasing thickness. The reduction of dimensions usually initiates strong fluctuations and suppresses correlations, therefore diminishing the coupling strength  $J$  of the exchange interactions, leading to the suppression of both Kondo and RKKY interaction. However, the magnitude of the impact can vary greatly. The resistance saturates slowly with decreasing thickness (SI), indicating the magnetic order overwhelms the Kondo interaction. In the 3 u.c. sample, the minimum in  $dR/dT$  disappears, leaving only a kink marked by a hollow triangle as the sole feature. Notably, we observe the emergence of magnetic ordered ground state in the 3 u.c. sample (Fig. 4b,c). The MR and transverse resistance  $R_{xy}$  both display hysteresis at 5 K, a phenomenon attributed to spin flipping. We further plot the MR and  $R_{xy}$  of the 11 u.c. sample with  $T_K$  at 16 K for comparison. The anomalous Hall effect is prominent in the  $R_{xy}$  of 4 u.c. sample but vanishes in the 11 u.c. one, indicating the strengthening of the magnetic ordered state controlled by dimensionality.

Figure 4d illustrates the temperature dependence of  $R_{xy}$  for the 4 u.c. sample. Both the magnitude of hysteresis and the anomalous Hall effect decrease as the temperature rises. We extract the anomalous Hall resistance  $R^{AHE}$  at zero field for each temperature and plot it in Fig. 4e together with  $R_{xx}$ . The consistency between the onset of  $R^{AHE}$  and the minimum of  $R_{xx}$  suggests that the origin of the magnetic order is the RKKY interaction introduced at  $T_N$ , which leads to an antiferromagnetic ordering.

The suppression of the  $T_K$  and strengthen of the antiferromagnetic order can be explained under the Doniach diagram, as shown in Fig. 5. The pink and blue dashed lines are the energy scales of Kondo interaction and RKKY interaction, respectively. The ground state is determined by mutual competition. In the orange regime, the comparable energy scale leads to the coexistence of two interactions, where the bulk CsCr<sub>6</sub>Sb<sub>6</sub> located. The suppression of  $J$  tuned by dimensional reduction push the system shift to left, where the Kondo interaction is drastically diminished and the transition temperature of AFM state is enhanced. As  $J$  is further reduced,  $T_N$  decreases proportionally with the RKKY interaction energy scale, as observed in the 3 u.c. sample with  $T_N$  at 40 K.

In conclusion, we aim to address the tunability of this Kagome materials using our newly discovered vdW Kagome antiferromagnet CsCr<sub>6</sub>Sb<sub>6</sub>. ARPES measurements reveals a clean flat band located 50 meV beneath the Fermi level, where the dominant contribution arises from the half-filled  $d_{xz}$  and  $d_{yz}$  orbitals of Cr. The intricate interaction of the flat band with the itinerant conduction sea is revealed through detailed transport measurements. The most prominent discovery is the realization of the Anomalous Hall

effect through exfoliation, indicating successful tuning of the Kondo interaction, which was previously difficult to achieve. Additionally, CsCr<sub>6</sub>Sb<sub>6</sub> is air stable and can be readily exfoliated into thin flakes, making it an excellent platform for incorporating various tuning methods such as electrical gating, stretching, bending, and heterostructuring.

## Reference

1. Stewart, G. R. Heavy-fermion systems. *Rev. Mod. Phys.* 56, 755–787 (1984).
2. Kirchner, S. et al. Colloquium: heavy-electron quantum criticality and single-particle spectroscopy. *Rev. Mod. Phys.* 92, 011002 (2020).
3. Paschen, S. & Si, Q. Quantum phases driven by strong correlations. *Nat. Rev. Phys.* 3, 9–26 (2021).
4. Coleman, P. Heavy fermions and the Kondo lattice: a 21st century perspective. Preprint at <https://arxiv.org/abs/1509.05769> (2015).
5. Kondo, J. Resistance Minimum in Dilute Magnetic Alloys. *Prog. Theor. Phys.* 32, 37 (1964).
6. Doniach, S. The Kondo lattice and weak antiferromagnetism. *Phys. B+C* 91, 231 (1977).
7. Si, Q. Quantum criticality and global phase diagram of magnetic heavy fermions. *Phys. Status Solidi* 247, 476–484 (2010).
8. Ernst, S. et al. Emerging local Kondo screening and spatial coherence in the heavy-fermion metal YbRh<sub>2</sub>Si<sub>2</sub>. *Nature* 474, 362–366 (2011).
9. Aynajian, P. et al. Visualizing heavy fermions emerging in a quantum critical Kondo lattice. *Nature* 486, 201–206 (2012).
10. Jiao, L. et al. Chiral superconductivity in heavy-fermion metal UTe<sub>2</sub>. *Nature* 579, 523–527 (2020).
11. Pfleiderer, C. et al. Partial order in the non-Fermi-liquid phase of MnSi. *Nature* 427, 227–231 (2004).
12. Stewart, G. R. Non-Fermi-liquid behavior in *d*- and *f*-electron metals. *Rev. Mod. Phys.* 73, 797–855 (2001).
13. Lohneysen, H. V., Rosch, A., Vojta, M. & Wolfle, P. Fermi-liquid instabilities at magnetic quantum phase transitions. *Rev. Mod. Phys.* 79, 1015–1075 (2007).
14. Gegenwart, P., Si, Q. & Steglich, F. Quantum criticality in heavy-fermion metals. *Nat. Phys.* 4, 186–197 (2008).
15. Aynajian, P. et al. Visualizing heavy fermions emerging in a quantum critical Kondo lattice. *Nature* 486, 201–206 (2012).
16. Allan, M. P. et al. Imaging Cooper pairing of heavy fermions in CeCoIn<sub>5</sub>. *Nat. Phys.* 9, 468–473 (2013).
17. Zhou, B. B. et al. Visualizing nodal heavy fermion superconductivity in CeCoIn<sub>5</sub>. *Nat. Phys.* 9, 474–479 (2013).
18. Vaño, V. et al. Artificial heavy fermions in a van der Waals heterostructure. *Nature* 599, 582–586 (2021).
19. Wen Wan. et al. Evidence for ground state coherence in a two-dimensional Kondo lattice. *Nat. Commun.* 14, 7005 (2023).
20. Wenjin Zhao. et al. Gate-tunable heavy fermions in a moiré Kondo lattice. *Nature* 616, 61–65 (2023).

21. Norman, M. R. Colloquium: Herbertsmithite and the search for the quantum spin liquid. *Rev. Mod. Phys.* **88**, 041002 (2016).
22. Kang, M. et al. Topological flat bands in frustrated kagome lattice CoSn. *Nat. Commun.* **11**, 4004 (2020).
23. Kang, M. et al. Dirac fermions and flat bands in the ideal Kagome metal FeSn. *Nat. Mater.* **19**, 163–169 (2020).
24. Guo, H. M. & Franz, M. Topological insulator on the kagome lattice. *Phys. Rev. B* **80**, 113102 (2009).
25. Ye, L. et al. Massive Dirac fermions in a ferromagnetic kagome metal. *Nature* **555**, 638–642 (2018).
26. Kang, M. et al. Twofold van Hove singularity and origin of charge order in topological kagome superconductor CsV<sub>3</sub>Sb<sub>5</sub>. *Nat. Phys.* **18**, 301–308 (2022).
27. Hu, Y. et al. Rich nature of Van Hove singularities in Kagome superconductor CsV<sub>3</sub>Sb<sub>5</sub>. *Nat. Commun.* **13**, 2220 (2022).
28. Linda Ye. et al. Hopping frustration-induced flat band and strange metallicity in a kagome metal. *Nat. Phys.* **20**, 610–614 (2024).
29. Songtian S. Zhang. et al. Many-body resonance in a correlated topological kagome antiferromagnet. Preprint at <https://arxiv.org/abs/2006.15770> (2020).

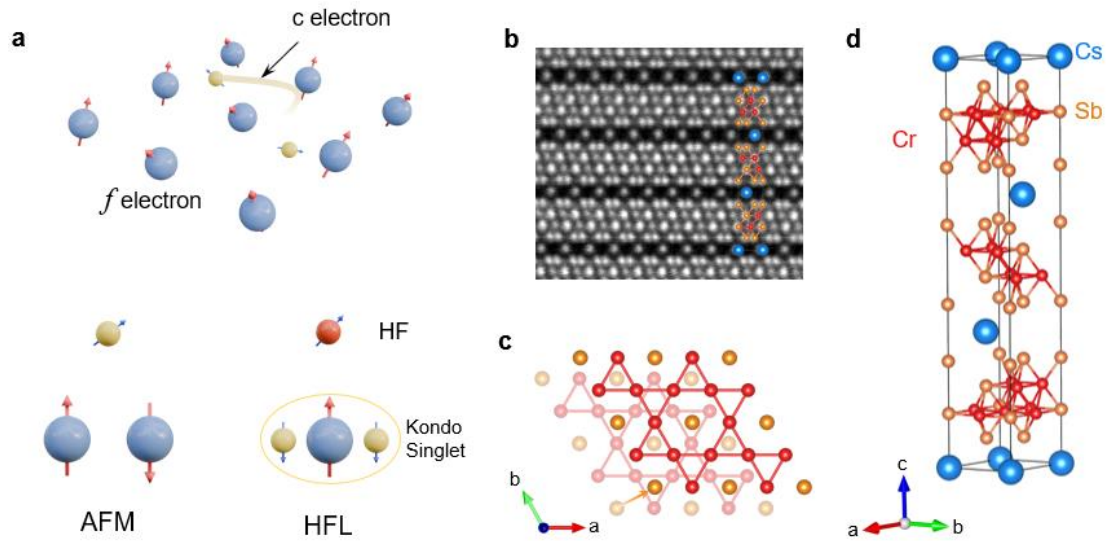


**Fig. 1 Kondo physics and crystal structure of  $\text{CsCr}_6\text{Sb}_6$ .** **a** sketches of conduction electrons scattered by local moments formed by  $f$ -electrons. At low temperature, two different ground states result from the RKKY and Kondo interactions by means of the scattering. **b** STEM image of  $\text{CsCr}_6\text{Sb}_6$ . the sample is fabricated by FIB to expose the crystal plane along  $a$  axis. The crystal structure superimposed on it is consistent well. **c**, **d** Crystal structure obtained from single crystal X-ray diffraction. Cs, Cr, Sb atoms are denoted by same color. A double Kagome structure sandwiched by Cs lattices are displayed from  $c$  axis in **c** with different transparency.



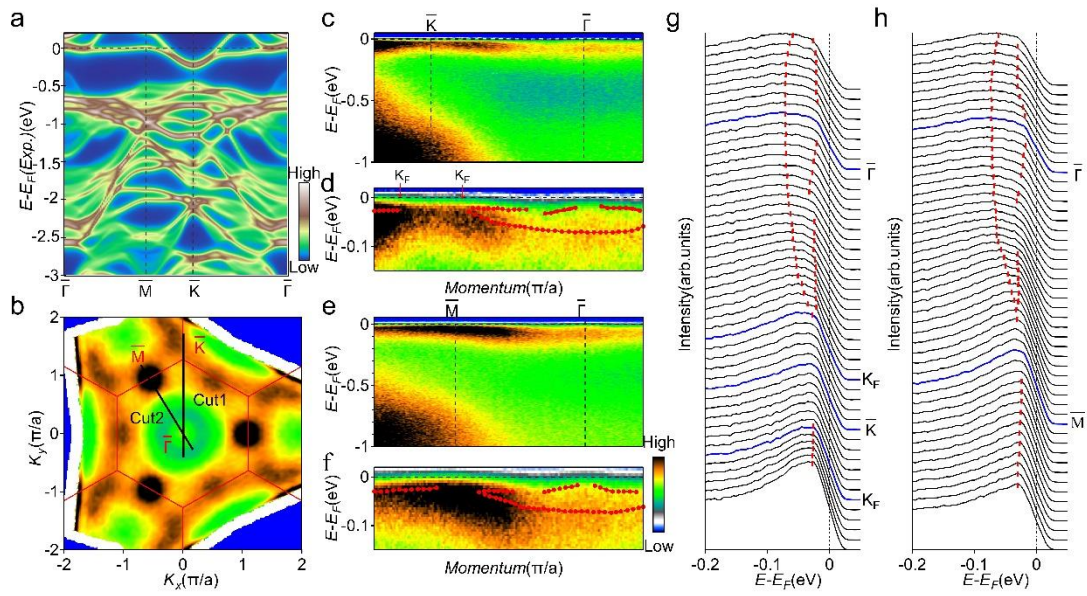


**Fig. 2 Hallmark of Kondo flat bands.** **a** Calculated bands dispersion based on the first principle DFT calculations. A flat band located at  $E_f$  except dispersion at  $K$  point. **b** Fermi surface mapping of CsCr<sub>6</sub>Sb<sub>6</sub> measured at a temperature of 15.5 K. It is obtained by integrating the spectral intensity within 10 meV with respect to the Fermi level and symmetrized assuming three-fold symmetry. **c**, **d** Detailed band structures measured along the  $\Gamma$ - K and  $\Gamma$ -M high symmetry directions based on He I lamp (21.2eV). **e**, **f** Photoemission spectra (EDCs) of CsCr<sub>6</sub>Sb<sub>6</sub> along the  $\Gamma$ - K and  $\Gamma$ -M high symmetry directions. The EDCs at  $K_F$ , K and M points are highlighted. The red tips mark the EDC peaks to trace the band dispersions.

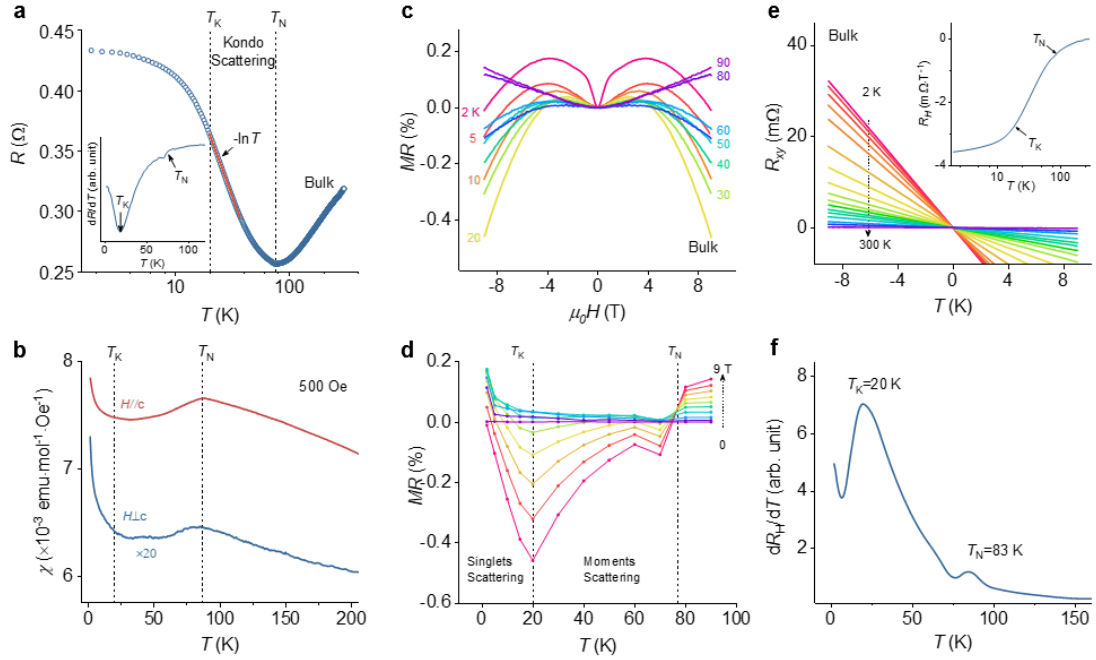


**Fig. 3 Formation of Kondo singlets.** **a** Resistance of bulk CsCr<sub>6</sub>Sb<sub>6</sub> sample. A minimum denoted as  $T_N$  is located at 78 K, below which the scattering of local moment leads to  $-\ln T$  dependence of the resistance. A deviation from  $-\ln T$  dependence at  $T_K$  marks the formation of Kondo singlets. **b** magnetic susceptibility  $\chi$  of CsCr<sub>6</sub>Sb<sub>6</sub> along and perpendicular to  $c$  axis. The drop at 80 K is related to the introduction of the RKKY interaction.  $\chi$  rise below  $T_K$ . **c** the normalized MR of CsCr<sub>6</sub>Sb<sub>6</sub> at various temperatures. **d** MR at different fields versus temperature, extracted from **c**. The magnetic response is divided to two regime by  $T_K$ . **e**  $R_{xy}$  of CsCr<sub>6</sub>Sb<sub>6</sub> at various temperature. No anomalous Hall effect emerges at all temperature. Inset is the extracted  $R_H$  through linear fitting, in which two kinks can be determined from **f**. **f** Differential  $R_H$  shows two peaks corresponding to  $T_K$  and  $T_N$ .

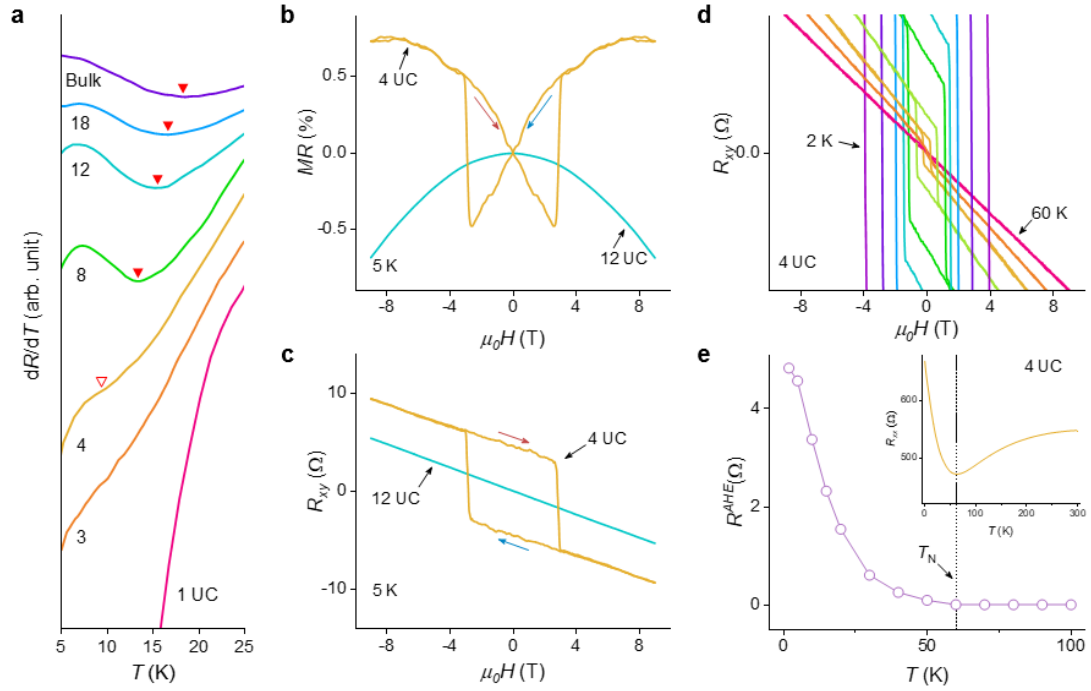


**Fig. 4 Tunable  $T_K$  and magnetic ground state.** **a**  $dR/dT$  of samples with different thickness from bulk to 1 UC. The data lines are renormalized and shifted comparing the minimum marking  $T_K$ .  $T_K$  is suppressed by the reduction of thickness significantly and vanishes in the 4 UC sample. **b** MR of two samples with thickness of 4 and a 12 UC, respectively. A hysteresis arises in the 4 UC sample. **c**  $R_{xy}$  of the 2 samples in **b**. a hysteresis accompanied with obvious anomalous Hall effect emerge in the 4 UC sample. **d** Temperature dependence of  $R_{xy}$  of the 4 UC sample. the anomalous Hall effect quenches at 60 K, consistent to the  $T_N$  defined by the minimum of the resistance in **e**.

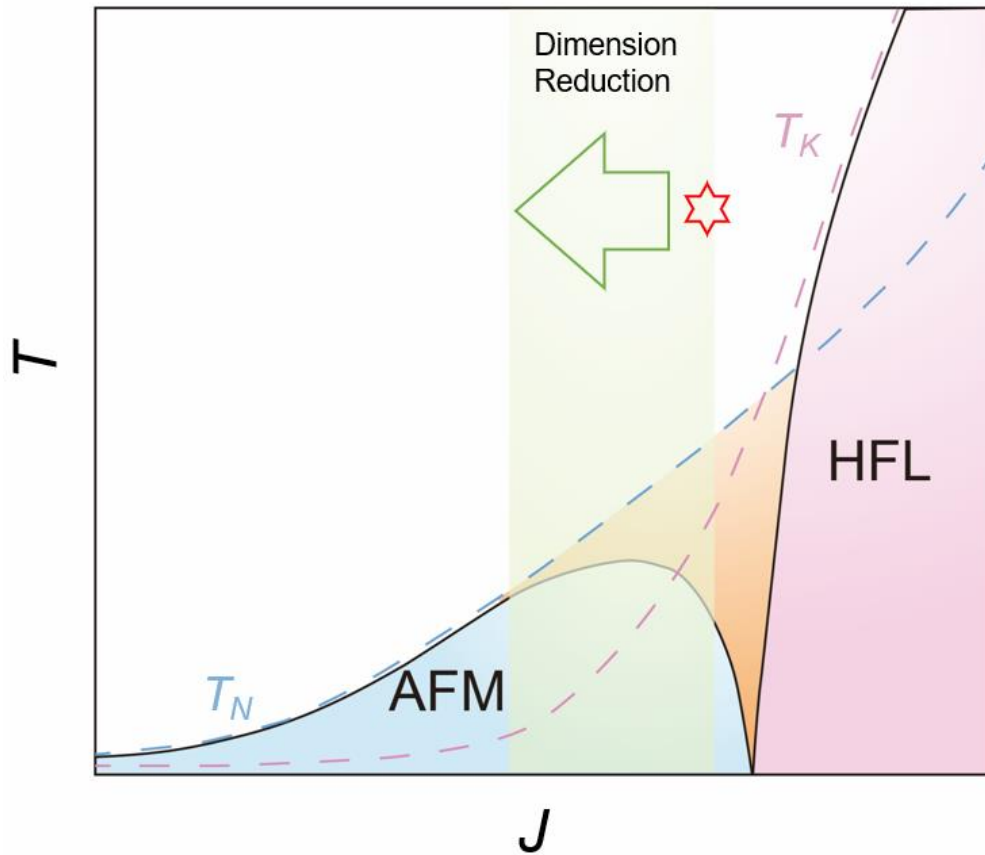


**Fig. 5 Dimensionality effect in a Doniach phase diagram.** Considering the energy scale  $T_N$  is larger than that  $T_K$  and the absence of magnetic ground state till 1.8 K, we suggest the bulk  $\text{CsCr}_6\text{Sb}_6$  located at left side near the QCP in the diagram. The dimensionality effect considerably suppressed the Kondo effect, leading to the enhancement of the AFM transition temperature to reach the RKKY energy scale  $T_N$  (blue broken curve).